

Excited State Absorption Drives Low-Energy Optical Limiting in Oligothiophenes

Mustapha Driouech,^{†,‡} Michele Guerrini,[‡] and Caterina Cocchi^{*,†,‡,¶}

[†]*Friedrich-Schiller Universität Jena, Institute for Condensed Matter Theory and Optics,
07743 Jena, Germany*

[‡]*Carl von Ossietzky Universität Oldenburg, Institute of Physics, 26129 Oldenburg, Germany*

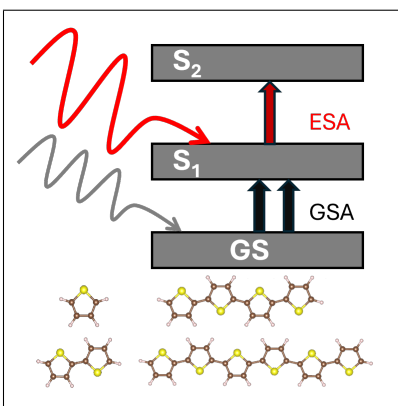
[¶]*Center for Nanoscale Dynamics (CeNaD), 26129 Oldenburg, Germany*

E-mail: caterina.cocchi@uni-jena.de

Abstract

Optical limiting (OL), a crucial mechanism for protecting human eyes and sensitive sensors from intense radiation, relies on understanding the optical nonlinearities acting on the systems. Assessing and disentangling the effects at play is crucial to predict and control the nonlinear optical response in real materials. In this *ab initio* study based on real-time time-dependent density-functional theory, we investigate non-perturbatively the absorption spectra of a set of thiophene oligomers, the building blocks of technologically relevant organic semiconductors, excited by broadband radiation of increasing intensity. Under strong electric fields, the absorption cross section grows significantly below the onset of linear excitations, exhibiting saturation typical of OL. By exciting the oligothiophenes with a train of pulses targeting the first and second excited states of each moiety and analyzing the resulting population dynamics, we reveal excited-state absorption (ESA) in the near-infrared to visible region. Our results indicate ESA as the driving mechanism for OL in oligothiophene molecules, thereby providing important insight to design novel compounds with optimized nonlinear optical characteristics.

TOC Graphic



Optical limiting (OL), the ability of a material to attenuate intense light transmission, is of critical importance for laser safety technologies,^{1,2} including the protection of sensitive optical sensors³ and human eyes.⁴⁻⁶ Designing efficient OL materials hinges on a fundamental understanding of the underlying optical nonlinearities. While mechanisms like reverse saturable absorption, excited-state absorption (ESA), and two-photon absorption are recognized as primary drivers of OL,⁷ identifying and disentangling their contributions in specific material classes remains a challenging task. Solving this conundrum is essential for advancing OL-based technologies.

Carbon-conjugated molecules have been intensively studied for OL due to their extended electronic π -network, large polarizability, and inherent chemical flexibility.⁸ Porphyrins and phthalocyanines have received significant attention, owing to their broad transparency window in the visible region that can be populated by intense radiation.^{9,10} While this interest has significantly promoted the study of OL and the development of applications,¹¹ it has diverted attention from other potentially relevant compounds, such as oligothiophene molecules. Their rich spectrum of linear excitations together with their tunability via chemical functionalization and length modulation¹²⁻¹⁴ have established them as building blocks for organic electronic devices.¹⁵⁻¹⁸ Although recent experimental studies on oligothiophene-functionalized graphene^{19,20} indicate their favorability for nonlinear optics and OL, the potential of oligothiophenes for this type of application remains largely unexplored. A detailed investigation of their response to strong fields is urgently needed to assess their ability as efficient OL compounds.

Ab initio methods are particularly well-suited for studying nonlinear optical properties of molecules. In contrast to empirical models, they do not require any input from experiments, thus representing a reliable and predictive tool to characterize new compounds. Real-time time-dependent density functional theory (RT-TDDFT), a non-perturbative first-principles approach, offers a particularly versatile framework. The “ δ -kick” method introduced by Yabana and Bertsch to simulate linear absorption spectra²¹ and subsequently extended to

probe nonlinear excitations driven by intense broadband radiation,²²⁻²⁴ is complemented by efficient schemes for pump-probe²⁵ and multidimensional spectroscopy²⁶ based on the application of pulsed electric fields of tunable shape, frequency, duration, and polarization, evolving with the system during a femtosecond (fs) time window.²⁷ This setup enables exploring dynamical charge transfer and non-equilibrium dynamics in organic, inorganic, and hybrid materials,²⁸⁻³⁶ including the influence of vibronic couplings when combined with Ehrenfest dynamics.³⁷⁻⁴⁰

In this work, we apply the δ -kick and pump-probe schemes of RT-TDDFT to investigate OL in four thiophene oligomers composed of 1, 2, 4, and 6 rings. By exciting the molecules with broadband radiation of increasing intensity, we find enhanced nonlinear absorption in the near-infrared to visible region below the onset of the linear spectrum. The saturation of this band upon increasing field intensity confirms its relation to OL. By impinging the oligothiophenes with a train of fs pulses and analyzing the resulting population dynamics, we rationalize their nonlinear optical behavior in terms of ESA. Our results have two important implications: they disclose the potential of oligothiophenes for OL in the near-infrared to visible region, depending on their length, and confirm the ability of RT-TDDFT to shed light on optical nonlinearities of conjugated molecules in an insightful and yet computationally efficient way.

We start our analysis by computing the absorption spectra of the four considered oligothiophenes applying δ -kicks of increasing intensity, ranging from a weak perturbation delivering the linear spectrum²¹ to strong fields triggering pronounced nonlinear response.²² The linear spectrum of the single thiophene ring (1T), obtained with a δ -kick of magnitude 0.001 \AA^{-1} , exhibits a peak around 5.5 eV (Figure 1a), which, due to intrinsic broadening (details in the Computational section) encompasses the two lowest-energy excitations polarized in the y - and x -direction, respectively⁴¹ (see Table S1 for the perturbative analysis of the linear excitations). Our findings are in very good agreement with quantum chemistry predictions^{42,43} and experimental results.^{44,45} Increasing the perturbation strength by two orders of mag-

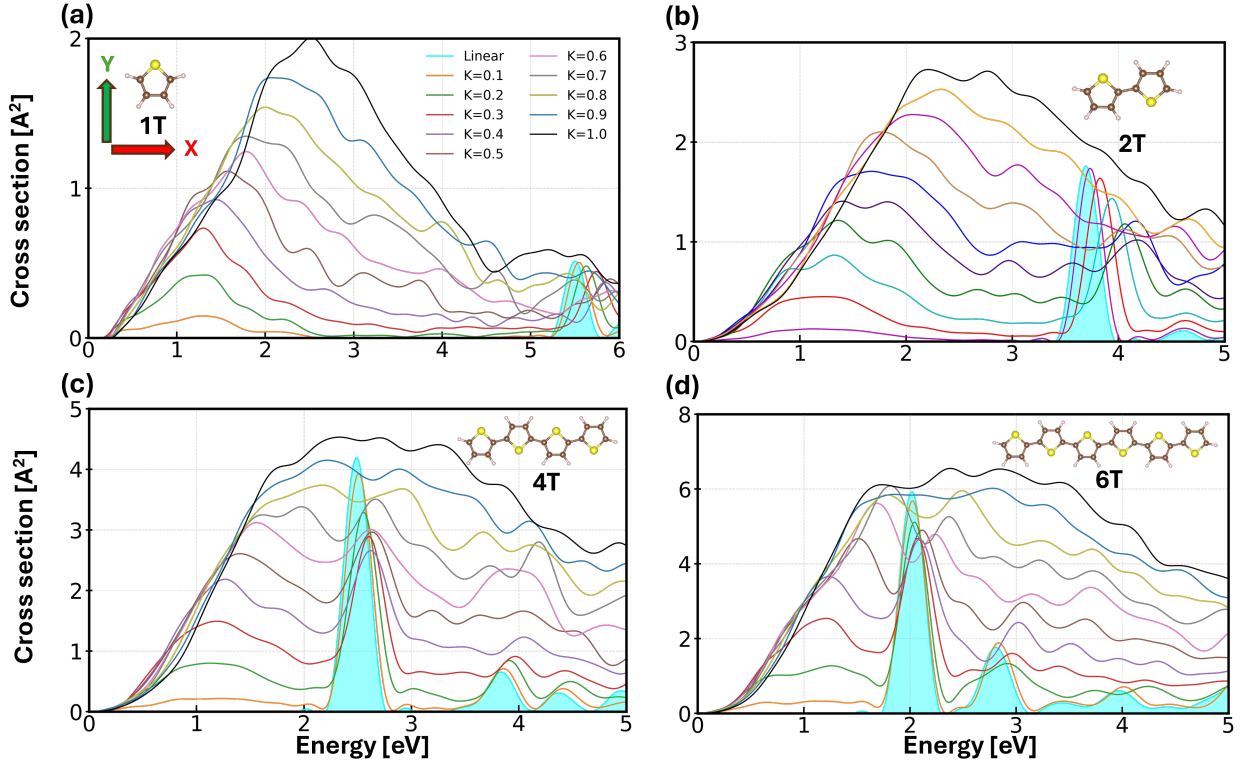


Figure 1: Absorption cross section computed for a) 1T, b) 2T, c) 4T, and d) 6T excited by instantaneous, broadband excitations of increasing intensities. Linear absorption spectra are obtained with a δ -kick of 0.001 \AA^{-1} (cyan filled areas), while nonlinear spectra are excited by kicks κ in \AA^{-1} specified in the legend of panel a). Insets: ball-and-stick representations of the investigated oligothiophene molecules with C atoms depicted in brown, S atoms in yellow, and H atoms in pink. The Cartesian coordinate system referred to all molecules is visualized in panel a).

nitude (δ -kick $\kappa = 0.1 \text{ \AA}^{-1}$) preserves the first absorption peak around 5.5 eV , but also leads to a non-zero cross section at low energies, between 0.5 and 2.5 eV . Larger values of the δ -kick induce a blue shift in the peak associated with the first linear excitation around 5.5 eV , a consequence of memory effects being neglected in the adopted adiabatic local density approximation.^{46,47} Importantly, the low-energy absorption band grows in intensity and further extends in energy with the magnitude of the kick, merging with the peak at 5.5 eV for $\kappa \geq 0.8 \text{ \AA}^{-1}$ (Figure 1a).

A similar behavior is exhibited by bithiophene (2T) under analogous excitation conditions. A weak δ -kick $\kappa = 0.001 \text{ \AA}^{-1}$ leads to the linear absorption spectrum of this molecule,

characterized by a sharp resonance around 3.8 eV (Figure 1b), in overall agreement with experiments^{45,48} and quantum-chemistry calculations.⁴⁹ Increasing the field intensity induces again a slight blue shift of the main absorption maximum due to the lack of memory effects in our calculations,^{46,47} and the appearance of a broad absorption band centered at 1 eV (Figure 1b). An even stronger perturbation shifts the maximum to 4 eV and further extends the energy range of the low-energy band across the entire visible range.

The linear absorption spectra of quaterthiophene (4T) and sexithiophene (6T) are characterized by strong resonances in the visible region, centered at approximately 2.5 eV (Figure 1c) and 2 eV (Figure 1d), respectively. These findings are in line with previous *ab initio* calculations^{50,51} and experiments.⁵²⁻⁵⁴ In the spectrum of 6T, a second weaker maximum appears at 2.8 eV. For 4T, this excitation has a lower oscillator strength and a higher energy, appearing at approximately 4 eV. In analogy with the shorter oligomers, perturbing these molecules with δ -kicks of increasing intensity promotes absorption in the low-energy spectral region, corresponding to infrared frequencies. The first absorption peak in the linear regime remains well-defined up to $\kappa = 0.4 \text{ \AA}^{-1}$, despite losing oscillator strength and being slightly blue-shifted (Figure 1c,d). In the spectrum of 4T, larger δ -kick intensities, up to $\kappa = 0.7 \text{ \AA}^{-1}$ enhance the spectral strength of this resonance while broadening it, while for $\kappa > 0.7 \text{ \AA}^{-1}$, a continuous absorption band rising at approximately 0.5 eV up to 4 eV is formed (Figure 1c). For 6T, the situation is more faceted. Kick strengths between 0.6 \AA^{-1} and 0.8 \AA^{-1} generate a two-peak structure in the absorption spectrum (Figure 1d), while, similar to 4T, stronger intensities give rise to featureless absorption from infrared to near-UV frequencies. The second absorption peak in the linear regime is more sensitive to the kick strength in the spectra of both molecules, where it is no longer distinguishable from $\kappa = 0.5 \text{ \AA}^{-1}$ in 4T (Figure 1c) and $\kappa = 0.6 \text{ \AA}^{-1}$ in 6T (Figure 1d).

The large low-energy absorption cross-section in the nonlinear spectra of the considered thiophene oligomers suggests the emergence of OL, further confirmed by its saturation upon integration in the relevant energy window (Figure S1). In contrast to phthalocyanine, where

the spectral window populated by intense, broadband radiation is identified between the two main absorption bands²² hosting dark transitions, enhanced nonlinear absorption in the spectra of oligothiophenes appears below the lowest-energy excitation in the linear regime. This finding suggests that ESA drives the response of these molecules to intense broadband radiation. To test this hypothesis, we perform an additional set of RT-TDDFT simulations, exciting the molecules with time-dependent pulses. By targeting the lowest-energy excitation ($S_0 \rightarrow S_1$, see Tables S1-S4 in the Supporting Information and the Computational Section below), we drive the molecules out of the linear regime. Next, we probe the population dynamics by impinging the moieties with a second pulse, delayed by 15 fs with respect to the first one and with carrier frequency in resonance with the low-absorption band emerging in the nonlinear regime.

The differential absorption spectra computed for each molecule after the application of the first pulse targeting $S_0 \rightarrow S_1$ are dominated by the excitation in resonance with the carrier frequency of the applied pulse (dashed vertical line in Figure 2). In addition, a weak but distinct absorption peak appears in the low-energy region of each spectrum, in the same window where strong δ -kicks give rise to non-zero absorption cross section (Figure 1). For 1T, this maximum appears in the visible region at 2.7 eV (Figure 2a), while for the longer oligomers, it is found at infrared frequencies, around 1 eV in 2T (Figure 2b), and close to 0.5 eV for both 4T (Figure 2c) and 6T (Figure 2d). The differential absorption spectra of the two longest molecules, 4T and 6T, are characterized by many more features compared to those of the shorter moieties. This is due to the higher density of excited states, which are involved in the nonlinear excitation. Nonetheless, all nonlinear spectra exhibit the same key characteristic, namely an absorption band in the near-infrared region, which is compatible with ESA.

To confirm this hypothesis, we monitor the electronic population dynamics by estimating the number of excited electrons through the contributions from time-dependent single-particle states $\phi_j(t)$, see Computational Section below, projected onto their ground-state

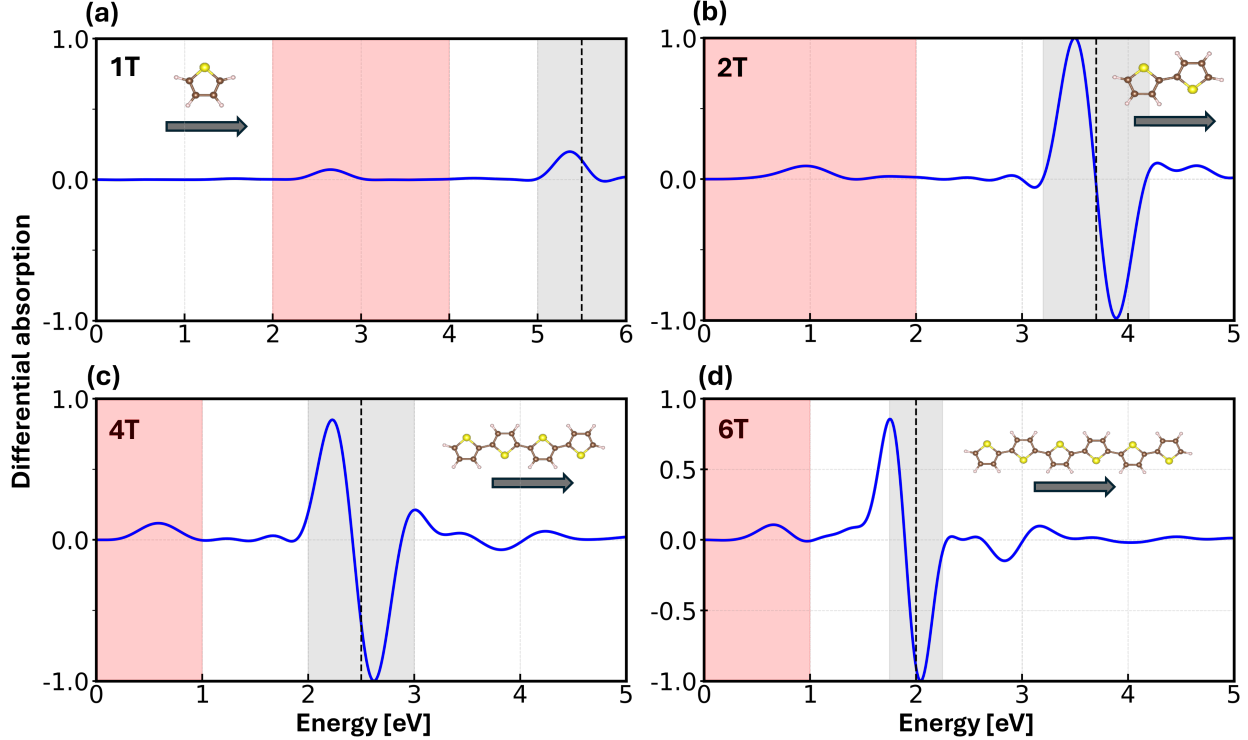


Figure 2: Differential absorption spectra of a) 1T, b) 2T, c) 4T, and d) 6T excited by a Gaussian pulse with peak intensity $I = 50 \text{ GW/cm}^2$ and photon energy of a) 5.5 eV, b) 3.7 eV, c) 2.5 eV, and d) 2.0 eV, in resonance with the first excitation in the linear spectra of the oligomers (dashed bars). The gray area indicates the bandwidth of the applied pulse, while the red shaded region highlights the low-energy nonlinear absorption band subsequently probed by the second pulse to access the population dynamics.

counterparts at $t = 0$:²⁵

$$N_{\text{ex}}(t) = 2 \sum_m^{\text{unocc}} \sum_j^{\text{occ}} |\langle \phi_m(0) | \phi_j(t) \rangle|^2, \quad (1)$$

where the pre-factor 2 accounts for spin degeneracy. We perform this analysis in two steps. Upon the application of the first pulse (gray area in Figure 3), which is set in resonance with the $S_0 \rightarrow S_1$ excitation in each molecule (gray area in Figure 2), we evaluate the amount of charge depleted from the ground state and promoted to the first excited state. In the single-particle framework provided by RT-TDDFT, we compute these contributions in terms of the occupation of the highest-occupied molecular orbital (HOMO) and the lowest-unoccupied molecular orbital (LUMO) involved in this transition, see Tables S1-S4. Next, we apply

a second pulse targeting the low-energy absorption maximum (red area in Figure 3) and estimate the number of electrons promoted from S_1 to higher excited states S_n , including contributions from LUMO+1 up to LUMO+10, see Figure S2.

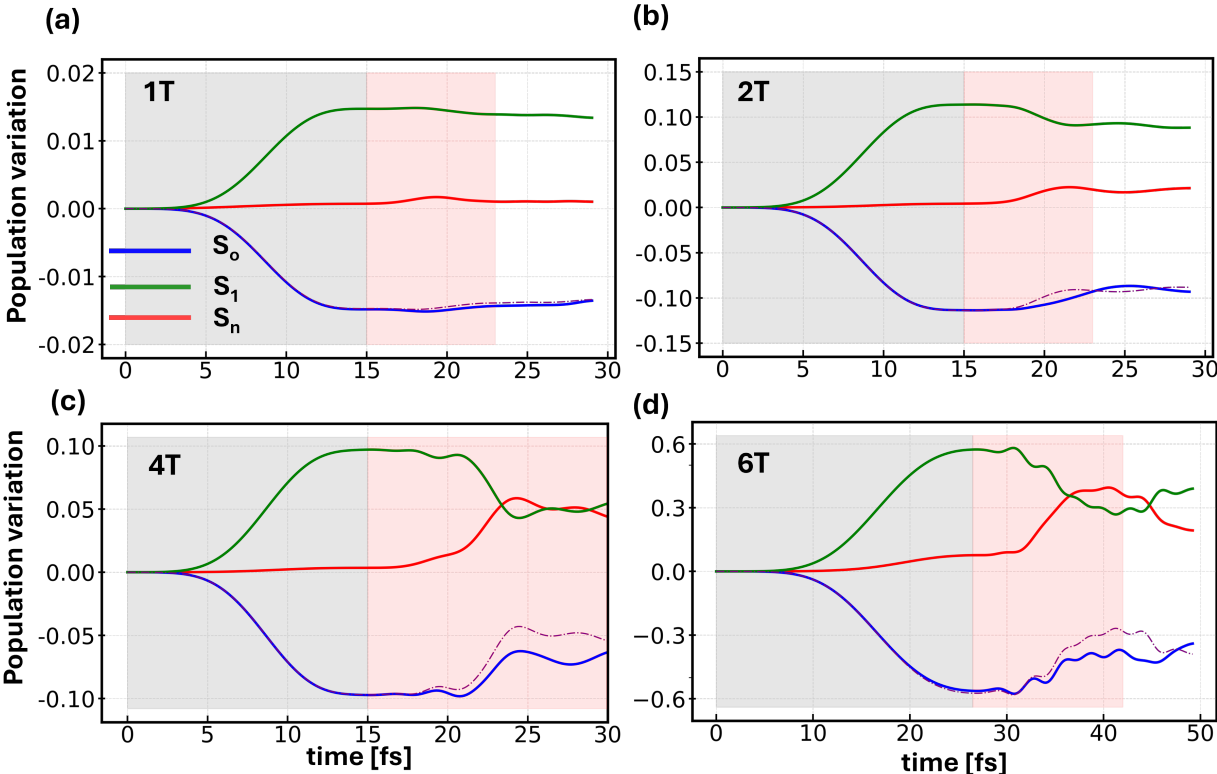


Figure 3: Variation in time of the population of the ground state (S_0) as well as of the first (S_1) and higher (single) excited states (S_n) of a) 1T, b) 2T, c) 4T, and d) 6T, driven by a train of two Gaussian pulses in resonance with the $S_0 \rightarrow S_1$ excitation (gray area) and with the absorption maximum below the linear onset (red area). The dotted-dashed purple line indicates the inverse of the population variation of S_1 .

The results visualized in Figure 3 validate our hypothesis regarding the role of ESA in driving low-energy nonlinear absorption in the oligothiophene molecules excited by strong broadband radiation. In 1T, the application of the first pulse with a carrier frequency of 5.5 eV triggers the occupation of S_1 at the expense of S_0 (Figure 3a, gray area). After 15 fs, when the second pulse with a carrier frequency of 3 eV is activated (Figure 3a, red area), we notice a slight reduction in S_1 due to the population of higher excited states (red curve). This is a signature of ESA. Concomitantly, the ground-state population rises, but without perfectly mirroring the S_1 population (dashed-dotted purple curve in Figure 3a), as during

the action of the first pulse. We attribute this behavior to ground-state bleaching during the population of excited states beyond S_1 .

In 2T, the mechanisms described above for 1T are amplified both quantitatively (compare the y -axis scale in Figure 3a and Figure 3b) and qualitatively. The first pulse with a carrier frequency of 3.7 eV shifts more than 0.1 e from the ground state to S_1 . After 20 fs, when the second pulse has reached its peak, the population of the first excitation decreases at the advantage of higher states (Figure 3b, red area). Again, signatures of a slight ground-state bleaching are visible through the mismatch between the blue solid curve and the dashed-dotted purple line in Figure 3b.

The situation is more faceted for 4T (Figure 3c). Here, the activation of the second pulse leads to a sizeable depletion of S_1 , which becomes less occupied than the other excited states after the second pulse has reached its peak. The S_n population receives non-negligible contributions also from the ground state, as indicated by the blue curve departing from the purple one, representing the inverse population of S_1 . In 6T, occupation variations become even larger in magnitude (Figure 3d) with S_1 losing more than 50% of the population gained from the first pulse during irradiation with the second. Higher excited states take up more than 30% of the total electronic population upon the application of the second pulse, with ground-state bleaching contributing to the process. It is worth noting that for 6T, excited states beyond S_1 are populated already by the first pulse (Figure 3d, gray area). The more elaborate composition of the first excited state in this long oligomer (see Table S4) likely plays a role here. However, we cannot exclude additional nonlinear effects emerging in the laser-driven dynamics, which will be investigated in follow-up work.

In summary, our RT-TDDFT simulations unambiguously attribute to ESA the absorption below the linear onset induced by intense, broadband radiation in the spectra of 1T, 2T, 4T, and 6T. This nonlinearity is associated with OL and discloses the potential of these molecules to be employed as active components for corresponding applications working in the near-infrared to visible region. We revealed this mechanism by exciting the systems with

a train of two pulses tuned in resonance with the first linear excitation in each molecule ($S_0 \rightarrow S_1$) and with transitions from the S_1 to higher excited states. The resulting electronic population dynamics support this interpretation, revealing ground-state depletion and the subsequent occupation of the first excited state under the action of the first pulse, as well as the population of higher excited states when the second pulse is turned on. While the length of the molecules and the consequent electronic-structure variations induce expected quantitative changes, the same qualitative behavior persists in the entire series, confirming ESA as the key mechanism driving OL in these compounds.

In conclusion, this study reveals the significant potential of oligothiophene molecules as OL compounds, featuring an active region in the near-infrared to visible band that effectively complements the window covered by more established materials like phthalocyanines and porphyrins. Our detailed analysis based on RT-TDDFT identifies ESA as the main driver of OL in these molecules. This work not only highlights the capability of this parameter-free, non-perturbative *ab initio* method to efficiently simulate and unveil the fundamental origins of optical nonlinearities in conjugated molecules but also sets the stage for the rational design of optimized OL compounds with in-depth insight into the underlying physical mechanisms.

Computational Methods

Theoretical Background

The calculations presented in this work are based on RT-TDDFT, based on the time propagation of the time-dependent Kohn-Sham (TDKS),

$$i\hbar \frac{\partial}{\partial t} \psi_i(\mathbf{r}, t) = \left(-\frac{\hbar^2}{2m} \nabla^2 + V_{\text{eff}}(\mathbf{r}, t) \right) \psi_i(\mathbf{r}, t), \quad (2)$$

where $\psi_i(\mathbf{r}, t)$ are the TDKS states and $V_{\text{eff}}(\mathbf{r}, t)$ is the time-dependent effective potential, including the contributions from the external potential, accounting for electron-nuclear inter-

actions, the Hartree potential, and the exchange-correlation potential. The time-dependent electron density, computed from the solution of the TDKS as $\rho(\mathbf{r}, t) = \sum_i^{occ} |\psi_i(\mathbf{r}, t)|^2$, enters the expression of the time-dependent transition dipole moment, which in the x -direction reads:

$$\langle x(t) \rangle = \int x \rho(\mathbf{r}, t) d\mathbf{r}. \quad (3)$$

The Fourier transform of Eq. (3),

$$\langle \tilde{x}(\omega) \rangle = \int \langle x(t) \rangle e^{i\omega t} dt, \quad (4)$$

is proportional to the polarizability α , whose imaginary part enters the expression of the absorption cross section.²¹

To compute the nonlinear response, we employed two computational approaches. In the so-called δ -kick scheme, introduced by Yabana and Bertsch²¹ and later applied by Cocchi *et al.* to simulate OL,²² the system is excited by an instantaneous broadband electric field, causing the electronic wave functions to acquire a phase factor expressed as $\psi_i(\mathbf{r}, t) \rightarrow \psi_i(\mathbf{r}, t)e^{i\kappa \cdot x}$ in the length gauge. The associated electric field is

$$\mathbf{E}(t) = \mathbf{E}_0 \delta(t), \quad (5)$$

with the amplitude $\mathbf{E}_0 = \frac{\hbar k}{e}$ depending linearly on the kick strength κ . The molecules are also excited with a time-dependent Gaussian-enveloped electric field of the form

$$\mathbf{E}(t) = \mathbf{E}_0 \exp \left[-\frac{(t - t_0)^2}{2\tau^2} \right] \cos(\omega_0 t), \quad (6)$$

where \mathbf{E}_0 is the peak amplitude, ω_0 the carrier frequency, t_0 the pulse center time, and τ the standard deviation related to the full-width half maximum of the Gaussian pulse indicated as the bandwidth of the laser in Figure 2.

Computational Details

All calculations reported in this work were performed with the code `octopus`,⁵⁵ implementing RT-TDDFT on real-space numerical grids. We adopted Troullier-Martins pseudopotentials⁵⁶ and the adiabatic local density approximation as implemented in the Perdew-Zunger functional.⁵⁷ The δ -kick simulations were carried out in a real-space box of size 15 Å and grid spacing of 0.18 Å. The TDKS equations were propagated using the enforced time-reversal symmetry propagator and Lanczos algorithm⁵⁸ with a time step of 10^{-3} fs = 1 as for a total duration of 15 fs, giving rise to an intrinsic broadening of 44 meV in the linear absorption spectra. The adopted δ -kicks were polarized in all three Cartesian directions to capture the full spectral response of the molecules. The electronic contributions to each linear excitation were resolved using the Casida method⁵⁹ (Tables S1-S4).

The runs with the Gaussian-shaped electric fields were carried out in a spherical box with a radius of 5 Å and grid spacing of 0.25 Å. The time-step is set to 2.9 as. To calculate the differential absorption (Figure 2), we excited 1T, 2T, and 4T with a pulse of peak intensity $I = 50$ GW/cm², while for 6T we took $I = 10$ GW/cm². The carrier frequencies were set in resonance with the $S_0 \rightarrow S_1$ transition of each molecule, namely 5.5 eV for 1T, 3.7 eV for 2T, 2.5 eV for 4T, and 2 eV for 6T. To amplify variations in the population dynamics (Figure 3), we applied the second pulse with a peak intensity of 2 TW/cm² for 1T and 2T, 1 TW/cm² for 4T, and 500 GW/cm² for 6T. The carrier frequency was set to 3 eV, 1 eV, 0.5 eV, and 0.5 eV for 1T, 2T, 4T, and 6T, respectively, targeting the absorption peak emerging in the differential absorption displayed in Figure 2.

Acknowledgement

C.C. acknowledges fruitful discussions with Carlo A. Rozzi in the preliminary stage of this project. This work was funded by the German Research Foundation, Project number 524452181, by the State of Lower Saxony (Professorinnen für Niedersachsen, DyNano,

and ELLiKo), and by the Federal Ministry of Education and Research (Professorinnenprogramm III). Computational resources were provided by the North-German Supercomputing Alliance (NHR), project nip00074.

Data Availability Statement

The data generated in this study, including the corresponding input files, are available free of charge on Zenodo, DOI: <https://doi.org/10.5281/zenodo.16037460> .

Supporting Information Available

In the Supporting Information, we report the integrated cross sections of the thiophene oligomers, the Casida analysis of their linear excitations, and the molecular orbital contributions to the population analysis.

References

- (1) Reena, P.; Joema, S.; Gunasekaran, B.; Sindhusha, S.; Girisun, T. S.; Darling, D. A. Scrutinizing the optical limiting action of a novel carbonyl guanidinium hippurate for laser safety device applications. *Opt. Mater.* **2022**, *132*, 112749.
- (2) T. C., S. G.; M, A. Genuine Two-Photon Absorption and Optical Limiting Property of the Ag-rGO-MoS2 Hybrid: Implications for Laser Safety Devices. *ACS Appl. Nano Mater.* **2024**, *7*, 3885–3896.
- (3) Hege, C.; Muller, O.; Merlat, L. Laser protection with optical limiting by combination of polymers with dyes. *J. Appl. Polym. Sci.* **2019**, *136*, 47150.
- (4) Grout, M. Application of bacteriorhodopsin for optical limiting eye protection filters. *Opt. Mater.* **2000**, *14*, 155–160.

- (5) Li, C.; Wang, R.; Liu, H.-K. Nonlinear optical limiters with grating sandwich structure for eye protection. *J. Nonlinear Opt. Phys. Mater.* **2000**, *9*, 413–422.
- (6) Muric, B. D.; Pantelic, D. V.; Vasiljevic, D. M.; Savic-Sevic, S. N.; Jelenkovic, B. M. Application of tot'hema eosin sensitized gelatin as a potential eye protection filter against direct laser radiation. *Current Appl. Phys.* **2016**, *16*, 57–62.
- (7) Tutt, L. W.; Boggess, T. F. A review of optical limiting mechanisms and devices using organics, fullerenes, semiconductors and other materials. *Prog. Quantum Electron.* **1993**, *17*, 299–338.
- (8) Sun, Y.-P.; Riggs, J. E. Organic and inorganic optical limiting materials. From fullerenes to nanoparticles. *Int. Rev. Phys. Chem.* **1999**, *18*, 43–90.
- (9) De La Torre, G.; Vázquez, P.; Agullo-Lopez, F.; Torres, T. Role of structural factors in the nonlinear optical properties of phthalocyanines and related compounds. *Chem. Rev.* **2004**, *104*, 3723–3750.
- (10) Calvete, M.; Yang, G. Y.; Hanack, M. Porphyrins and phthalocyanines as materials for optical limiting. *Synth. Met.* **2004**, *141*, 231–243.
- (11) Liu, Z.; Zhang, B.; Chen, Y. Recent progress in two-dimensional nanomaterials for laser protection. *Chemistry* **2019**, *1*, 17–43.
- (12) Salzner, U. Theoretical investigation of excited states of oligothiophenes and of their monocations. *J. Chem. Theory. Comput.* **2007**, *3*, 1143–1157.
- (13) Badaeva, E.; Harpham, M. R.; Guda, R.; Suzer, O.; Ma, C.-Q.; Bauerle, P.; Goodson III, T.; Tretiak, S. Excited-state structure of oligothiophene dendrimers: Computational and experimental study. *J. Phys. Chem. B* **2010**, *114*, 15808–15817.
- (14) Krumland, J.; Valencia, A. M.; Cocchi, C. Exploring organic semiconductors in solution:

- the effects of solvation, alkylation, and doping. *Phys. Chem. Chem. Phys.* **2021**, *23*, 4841–4855.
- (15) Sakai, J.; Taima, T.; Saito, K. Efficient oligothiophene: fullerene bulk heterojunction organic photovoltaic cells. *Org. Electron.* **2008**, *9*, 582–590.
- (16) Xia, Q.; Burkhardt, M.; Halik, M. Oligothiophenes in organic thin film transistors—Morphology, stability and temperature operation. *Org. Electron.* **2008**, *9*, 1061–1068.
- (17) Yang, K.; Chen, Z.; Wang, Y.; Guo, X. Alkoxy-functionalized bithiophene/thiazoles: versatile building blocks for high-performance organic and polymeric semiconductors. *Acc. Mater. Res.* **2023**, *4*, 237–250.
- (18) Zaier, R.; Martel, A.; Antosiewicz, T. J. Effect of benzothiadiazole-based π -spacers on fine-tuning of optoelectronic properties of oligothiophene-core donor materials for efficient organic solar cells: a DFT study. *J. Phys. Chem. A* **2023**, *127*, 10555–10569.
- (19) Liu, Y.; Zhou, J.; Zhang, X.; Liu, Z.; Wan, X.; Tian, J.; Wang, T.; Chen, Y. Synthesis, characterization and optical limiting property of covalently oligothiophene-functionalized graphene material. *Carbon* **2009**, *47*, 3113–3121.
- (20) Midya, A.; Mamidala, V.; Yang, J.-X.; Ang, P. K. L.; Chen, Z.-K.; Ji, W.; Loh, K. P. Synthesis and superior optical-limiting properties of fluorene-thiophene-benzothiadazole polymer-functionalized graphene sheets. *Small* **2010**, *6*, 2292–2300.
- (21) Yabana, K.; Bertsch, G. F. Time-dependent local-density approximation in real time. *Phys. Rev. B* **1996**, *54*, 4484–4487.
- (22) Cocchi, C.; Prezzi, D.; Ruini, A.; Molinari, E.; Rozzi, C. A. Ab initio simulation of optical limiting: the case of metal-free phthalocyanine. *Phys. Rev. Lett.* **2014**, *112*, 198303.

- (23) Fischer, S. A.; Cramer, C. J.; Govind, N. Excited-state absorption from real-time time-dependent density functional theory: Optical limiting in zinc phthalocyanine. *J. Phys. Chem. Lett.* **2016**, *7*, 1387–1391.
- (24) Guandalini, A.; Cocchi, C.; Pittalis, S.; Ruini, A.; Rozzi, C. A. Nonlinear light absorption in many-electron systems excited by an instantaneous electric field: a non-perturbative approach. *Phys. Chem. Chem. Phys.* **2021**, *23*, 10059–10069.
- (25) Krumland, J.; Valencia, A. M.; Pittalis, S.; Rozzi, C. A.; Cocchi, C. Understanding real-time time-dependent density-functional theory simulations of ultrafast laser-induced dynamics in organic molecules. *J. Chem. Phys.* **2020**, *153*, 054106.
- (26) Krumland, J.; Guerrini, M.; De Sio, A.; Lienau, C.; Cocchi, C. Two-dimensional electronic spectroscopy from first principles. *Appl. Phys. Rev.* **2024**, *11*, 011305.
- (27) De Giovannini, U.; Brunetto, G.; Castro, A.; Walkenhorst, J.; Rubio, A. Simulating pump-probe photoelectron and absorption spectroscopy on the attosecond timescale with time-dependent density functional theory. *ChemPhysChem* **2013**, *14*, 1363–1376.
- (28) Zhang, J.; Hong, H.; Lian, C.; Ma, W.; Xu, X.; Zhou, X.; Fu, H.; Liu, K.; Meng, S. Interlayer-state-coupling dependent ultrafast charge transfer in MoS₂/WS₂ bilayers. *Adv. Sci.* **2017**, *4*, 1700086.
- (29) Lian, C.; Guan, M.; Hu, S.; Zhang, J.; Meng, S. Photoexcitation in solids: First-principles quantum simulations by real-time TDDFT. *Adv. Theory Simul.* **2018**, *1*, 1800055.
- (30) Jacobs, M.; Krumland, J.; Valencia, A. M.; Wang, H.; Rossi, M.; Cocchi, C. Ultrafast charge transfer and vibronic coupling in a laser-excited hybrid inorganic/organic interface. *Adv. Phys. X* **2020**, *5*, 1749883.

- (31) Neufeld, O.; Tancogne-Dejean, N.; De Giovannini, U.; Hübener, H.; Rubio, A. Light-Driven Extremely Nonlinear Bulk Photogalvanic Currents. *Phys. Rev. Lett.* **2021**, *127*, 126601.
- (32) Liu, Z.; Wang, F.; Sheng, X.; Wang, J.; Jiang, L.; Wei, Z. Ultrafast response of cubic silicon carbide to intense attosecond pulse light. *Phys. Rev. B* **2021**, *104*, 064103.
- (33) Uemoto, M.; Kurata, S.; Kawaguchi, N.; Yabana, K. First-principles study of ultrafast and nonlinear optical properties of graphite thin films. *Phys. Rev. B* **2021**, *103*, 085433.
- (34) Jacobs, M.; Krumland, J.; Cocchi, C. Laser-controlled charge transfer in a two-dimensional organic/inorganic optical coherent nanojunction. *ACS Appl. Nano Mater.* **2022**, *5*, 5187–5195.
- (35) Uratani, H.; Nakai, H. Nanoscale and real-time nuclear–electronic dynamics simulation study of charge transfer at the donor–acceptor interface in organic photovoltaics. *J. Phys. Chem. Lett.* **2023**, *14*, 2292–2300.
- (36) Qi, H.; Wang, J.; Xu, Z.; Fang, F. First-principles study of electron dynamics of MoS₂ under femtosecond laser irradiation from deep ultraviolet to near-infrared wavelengths. *J. Chem. Phys.* **2024**, *161*, 224709.
- (37) Jacobs, M.; Krumland, J.; Valencia, A. M.; Cocchi, C. Pulse-induced dynamics of a charge-transfer complex from first principles. *J. Phys. Chem. A* **2023**, *127*, 8794–8805.
- (38) Guerrini, M.; Krumland, J.; Cocchi, C. Vibronic dynamics from real-time time-dependent density-functional theory coupled to the Ehrenfest scheme: the example of p-coumaric acid. *Theor. Chem. Acta* **2023**, *142*, 110.
- (39) Jacobs, M.; Fidanyan, K.; Rossi, M.; Cocchi, C. Impact of nuclear effects on the ultrafast dynamics of an organic/inorganic mixed-dimensional interface. *Electron. Struct.* **2024**, *6*, 025006.

- (40) Xu, J.; Zhou, R.; Li, T. E.; Hammes-Schiffer, S.; Kanai, Y. Lagrangian formulation of nuclear–electronic orbital Ehrenfest dynamics with real-time TDDFT for extended periodic systems. *J. Chem. Phys.* **2024**, *161*, 194109.
- (41) Cocchi, C.; Draxl, C. Optical spectra from molecules to crystals: Insight from many-body perturbation theory. *Phys. Rev. B* **2015**, *92*, 205126.
- (42) Salzmann, S.; Kleinschmidt, M.; Tatchen, J.; Weinkauff, R.; Marian, C. M. Excited states of thiophene: ring opening as deactivation mechanism. *Phys. Chem. Chem. Phys.* **2008**, *10*, 380–392.
- (43) Kölle, P.; Schnappinger, T.; de Vivie-Riedle, R. Deactivation pathways of thiophene and oligothiophenes: internal conversion versus intersystem crossing. *Phys. Chem. Chem. Phys.* **2016**, *18*, 7903–7915.
- (44) Holland, D.; Trofimov, A.; Seddon, E.; Gromov, E.; Korona, T.; De Oliveira, N.; Archer, L.; Joyeux, D.; Nahon, L. Excited electronic states of thiophene: high resolution photoabsorption Fourier transform spectroscopy and ab initio calculations. *Phys. Chem. Chem. Phys.* **2014**, *16*, 21629–21644.
- (45) Haberkern, H.; Asmis, K. R.; Allan, M.; Swiderek, P. Triplet states in oligomeric materials: Electron energy loss spectroscopy of thiophene and bithiophene and extrapolation to the polymer. *Phys. Chem. Chem. Phys.* **2003**, *5*, 827–833.
- (46) Wijewardane, H. O.; Ullrich, C. A. Real-Time Electron Dynamics with Exact-Exchange Time-Dependent-Density-Functional Theory. *Phys. Rev. Lett.* **2008**, *100*, 056404.
- (47) Fuks, J. I.; Helbig, N.; Tokatly, I. V.; Rubio, A. Nonlinear phenomena in time-dependent density-functional theory: What Rabi oscillations can teach us. *Phys. Rev. B* **2011**, *84*, 075107.

- (48) Lap, D.; Grebner, D.; Rentsch, S. Femtosecond time-resolved spectroscopic studies on thiophene oligomers. *J. Phys. Chem. A* **1997**, *101*, 107–112.
- (49) Andrzejak, M.; Witek, H. A. The elusive excited states of bithiophene: a CASPT2 detective story. *Theor. Chem. Acta* **2011**, *129*, 161–172.
- (50) Leng, X.; Yin, H.; Liang, D.; Ma, Y. Excitons and Davydov splitting in sexithiophene from first-principles many-body Green’s function theory. *J. Chem. Phys.* **2015**, *143*, 114501.
- (51) Sun, S.-m.; Zhang, S.; Liu, K.; Wang, Y.-p.; Zhang, B. The geometry relaxation and intersystem crossing of quaterthiophene studied by femtosecond spectroscopy. *Photochem. Photobiol. Sci.* **2015**, *14*, 853–858.
- (52) Birnbaum, D.; Fichou, D.; Kohler, B. E. The lowest energy singlet state of tetrathio-
phene, an oligomer of polythiophene. *J. Chem. Phys.* **1992**, *96*, 165–169.
- (53) Yang, A.; Kuroda, M.; Shiraishi, Y.; Kobayashi, T. Chain-length dependent stationary and time-resolved spectra of α -oligothiophenes. *J. Phys. Chem. B* **1998**, *102*, 3706–3711.
- (54) Rentsch, S.; Yang, J. P.; Paa, W.; Birckner, E.; Schiedt, J.; Weinkauff, R. Size dependence of triplet and singlet states of α -oligothiophenes. *Phys. Chem. Chem. Phys.* **1999**, *1*, 1707–1714.
- (55) Tancogne-Dejean, N.; Oliveira, M. J. T.; Andrade, X.; Appel, H.; Borca, C. H.; Le Breton, G.; Buchholz, F.; Castro, A.; Corni, S.; Correa, A. A. et al. Octopus, a computational framework for exploring light-driven phenomena and quantum dynamics in extended and finite systems. *J. Chem. Phys.* **2020**, *152*, 124119.
- (56) Troullier, N.; Martins, J. L. Efficient pseudopotentials for plane-wave calculations. *Phys. Rev. B* **1991**, *43*, 1993–2006.

- (57) Perdew, J. P.; Zunger, A. Self-interaction correction to density-functional approximations for many-electron systems. *Phys. Rev. B* **1981**, *23*, 5048–5079.
- (58) Lanczos, C. An iteration method for the solution of the eigenvalue problem of linear differential and integral operators. *J. Res. Natl. Bur. Stand. B* **1950**, *45*, 255–282.
- (59) Casida, M. E.; Jamorski, C.; Casida, K. C.; Salahub, D. R. Molecular excitation energies to high-lying bound states from time-dependent density-functional response theory: Characterization and correction of the time-dependent local density approximation ionization threshold. *J. Chem. Phys.* **1998**, *108*, 4439–4449.